

Spaser quenching and mode mixing in plasmonic systems with gain

L. S. Petrosyan and T. V. Shahbazyan

Department of Physics, Jackson State University, Jackson MS 39217 USA

We study the effect of off-resonance plasmon modes on spaser action in plasmonic systems with gain. We show that mode mixing originates from inhomogeneity of gain distribution near the metal surface and leads to an upward shift of spaser frequency and population inversion threshold. This effect is similar, albeit significantly weaker, to quenching of plasmon-enhanced fluorescence of a single emitter near metal nanostructure due to excitation of nonresonant modes with wide spectral band. We also show that spaser quenching is suppressed for large gain concentrations, and establish a simple criteria for quenching onset, which we support by numerical calculations for spherical geometry.

PACS numbers: 78.67.Bf, 73.20.Mf, 33.20.Fb, 33.50.-j

I. INTRODUCTION

The prediction of plasmonic laser (spaser) [1–3] and its experimental realization in various systems [4–14] have been among the highlights in the rapidly developing field of plasmonics during past decade [15]. First observed in gold nanoparticles (NP) coated by dye-doped silica shells [4], spaser action was reported in hybrid plasmonic waveguides [5], semiconductor quantum dots on metal film [6, 12], plasmonic nanocavities and nanocavity arrays [7–10, 13, 14], metallic NP and nanorods [4, 11], and more recently, carbon-based structures [16, 17] and hyperbolic materials [18]. Small spaser size well below the diffraction limit gives rise to wealth of promising applications [19].

The spaser feedback mechanism is based on energy transfer (ET) between quantum emitters (QE), constituting gain medium, and resonant plasmon mode. Even though a metal nanostructure usually possesses discrete spectrum of localized plasmon modes, e.g., characterized by angular momentum l for spherical systems, the QE coupling to *nonresonant* modes with well separated frequencies is typically considered sufficiently weak to be neglected. However, this is a good approximation for high quality cavity modes, while plasmon resonances are characterized by much broader lineshape due to large Ohmic losses in metal, so that a significant fraction of QE energy is transferred to nonresonant modes at small QE distances to the metal surface, where the coupling to nonresonant modes is large [20–23]. During past decade, numerous experiments reported plasmon-enhanced fluorescence of dye molecules or semiconductor quantum dots near metal NPs which, however, was quenched as QEs moved closer to the NP surface [24–50]. Fluorescence quenching in plasmonic systems is best illustrated by distance dependency of quantum efficiency $Q = \Gamma_r / (\Gamma_r + \Gamma_{nr})$ of a radiating dipole with frequency tuned to the dipole plasmon resonance in spherical metal NP (see Fig. 1). Here Γ_r is plasmon-enhanced radiative decay rate and Γ_{nr} is nonradiative decay rate due to QE coupling to high- l nonresonant modes (see below for detail). With decreasing QE-NP distance d , nonradiative QE decay into nonreso-

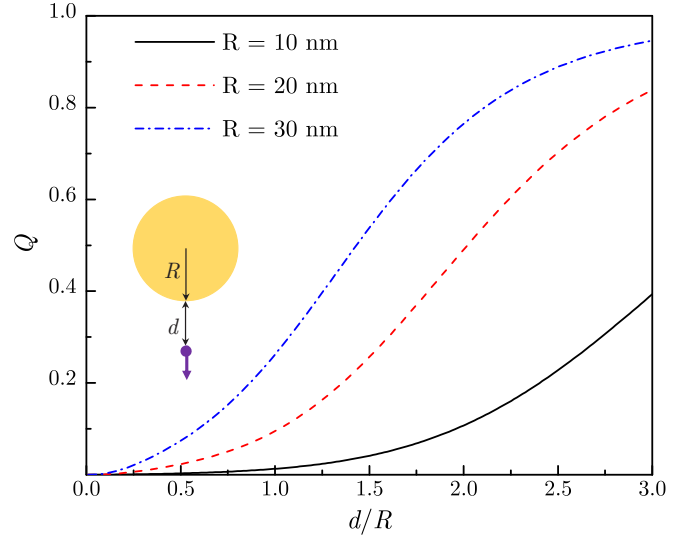


FIG. 1. Fluorescence quantum efficiency for a QE near spherical Au NP is shown vs. QE-NP distance for several NP sizes.

nant modes dominates, so that, for distances comparable to NP radius R , the quantum efficiency is low.

In plasmonic systems with gain, the effect of gain coupling to nonresonant modes is twofold. First, QEs coupling to higher-order plasmons (with higher frequencies) should lead to upward shift of spaser frequency, and, second, the energy transfer (ET) from QEs to nonresonant modes can interfere with the feedback mechanism, resulting in higher population inversion threshold. Both effects have increasingly negative impact on spaser action as the (average) distance between QEs and the metal surface is reduced, which raises the issue of *spaser quenching* for substantially close gain-metal proximity. While spaser action has been modeled in a number of specific systems [3, 51–55], little work has been done on the role of nonresonant modes. A recent numerical study involving core-shell NP indicated limited impact of nonresonant modes on the spaser action [56]. However, no comprehensive study on the role of nonresonant modes in spaser action has so far been carried out.

The goal of this paper is to develop an analytical model for plasmonic systems with gain that includes gain cou-

pling to nonresonant modes, and to establish criteria for spaser quenching. We show that inhomogeneity of gain distribution near the metal surface gives rise to plasmon mode mixing leading to increase of spaser frequency and population and population inversion threshold. However, with increasing gain concentration, role of nonresonant modes in spaser action is reduced and their overall effect is much weaker in plasmon-enhanced fluorescence. For NP-based spasers, we obtain a simple condition for spaser quenching onset, which we support by numerical calculations.

The paper is organized as follows. In the Sec. II, we set up Maxwell-Bloch equation for pumped QEs interacting with a composite spherical NP. In Sec. III, we introduce system collective modes and show that mode mixing originates from inhomogeneity of gain distribution. In Sec. IV, we study the effect of mode mixing on spaser condition, and obtain a simple criteria for spaser onset supported by numerical calculations. We summarize our findings in Sec. V, and provide some technical detail in the Appendices.

II. PUMPED QUANTUM EMITTERS INTERACTING WITH A METAL NANOPARTICLE

We consider a thin layer of M QEs randomly distributed on top of a spherical core-shell NP with metal core of radius R and a dielectric shell of uniform thickness d . Within semiclassical approach, electromagnetic fields are treated classically, while QEs are described by pumped two-level systems located at \mathbf{r}_j with excitation frequency ω_{12} between energy levels 1 and 2. Each QE is characterized by polarization $\rho_j \equiv \rho_{12}^{(j)}$ and occupation $n_j \equiv \rho_{22}^{(j)} - \rho_{11}^{(j)}$, where $\rho_{ab}^{(j)}$ ($a, b = 1, 2$) is the density matrix for j th QE. The ensemble population inversion is $N = \sum_j n_j$. In the rotating wave approximation, the steady-state dynamics of QEs coupled to alternating electric field $\mathcal{E}(\mathbf{r})e^{-i\omega t}$ is described by the standard Maxwell-Bloch equations

$$(\omega - \omega_{21} + i/\tau_2) \rho_j = \frac{\mu}{\hbar} n_j \mathbf{e}_j \cdot \mathcal{E}(\mathbf{r}_j), \quad (1)$$

$$n_j - \bar{n} = -\frac{4\mu\tau_1}{\hbar} \text{Im}[\rho_j \mathbf{e}_j \cdot \mathcal{E}(\mathbf{r}_j)],$$

where τ_2 and τ_1 are time constants characterizing polarization and population relaxation, μ and \mathbf{e}_j are, respectively, the QE dipole matrix element and orientation, and \bar{n} is the average population inversion per QE due to the pump. The local field $\mathcal{E}(\mathbf{r}_j)$ is generated by all QEs' dipole moments $\mathbf{p}_j = \mu \mathbf{e}_j \rho_j$ and, within semiclassical approach, has the form

$$\mathcal{E}(\mathbf{r}_j) = \frac{4\pi\omega^2}{c^2} \sum_k \bar{\mathbf{G}}(\omega; \mathbf{r}_j, \mathbf{r}_k) \cdot \mathbf{p}_k, \quad (2)$$

where $\bar{\mathbf{G}}(\omega; \mathbf{r}, \mathbf{r}')$ is the electromagnetic Green dyadic in the presence of metal nanostructure and c is the speed

of light. Using Eq. (2) to eliminate the electric field, the system (1) takes the form

$$\sum_{k=1}^M \left[\left(\omega - \omega_{21} + \frac{i}{\tau_2} \right) \delta_{jk} - \frac{\mu^2}{\hbar} n_j D_{jk} \right] \rho_j = 0, \\ n_j - \bar{n} + \frac{4\tau_1\mu^2}{\hbar} \text{Im} \sum_{k=1}^M (\rho_j^* D_{jk} \rho_j) = 0, \quad (3)$$

where δ_{jk} is Kronecker symbol and $D_{jk}(\omega)$ is a frequency-dependent coupling matrix in position space,

$$D_{jk}(\omega) = \frac{4\pi\omega^2}{c^2} \mathbf{e}_j \cdot \bar{\mathbf{G}}(\omega; \mathbf{r}_j, \mathbf{r}_k) \cdot \mathbf{e}_k. \quad (4)$$

Below the diffraction limit, the Green dyadic can be replaced by its near-field limit, and the coupling matrix (4) represents a sum of direct and plasmon terms, $D_{jk} = D_{jk}^0 + D_{jk}^p$, which, for spherical geometry, are given by multipole expansions [22, 23]

$$D_{jk}^0 = -\sum_{lm} \left[\psi_{lm}^{(j)} \chi_{lm}^{(k)*} \theta_{jk} + \chi_{lm}^{(j)} \psi_{lm}^{(k)*} \theta_{kj} \right], \\ D_{jk}^p = \sum_{lm} \alpha_l \psi_{lm}^{(j)} \psi_{lm}^{(k)*}, \quad (5)$$

where l and m are the polar and azimuthal numbers, respectively, and $\theta_{jk} \equiv \theta(r_j - r_k)$ is the step-function. Here, $\alpha_l(\omega)$ is l -pole polarizability for a spherical NP in a medium with dielectric constant ε_d ,

$$\alpha_l(\omega) = \frac{R^{2l+1}(\varepsilon - \varepsilon_d)}{\varepsilon + (1 + l^{-1})\varepsilon_d}, \quad (6)$$

where $\varepsilon(\omega)$ is the metal dielectric function, and the basis functions are given by

$$\chi_{lm}^{(j)} = C_l \mathbf{e}_j \cdot \nabla_j [r_j^l Y_{lm}(\hat{\mathbf{r}}_j)], \quad \psi_{lm}^{(j)} = C_l \mathbf{e}_j \cdot \nabla_j \left[\frac{Y_{lm}(\hat{\mathbf{r}}_j)}{r_j^{l+1}} \right], \quad (7)$$

where $C_l = \sqrt{4\pi/(2l+1)}$ is normalization coefficient and $Y_{lm}(\hat{\mathbf{r}})$ are the spherical harmonics. The basis functions satisfy orthogonality relations

$$\langle \chi_{lm}^{(j)*} \chi_{l'm'}^{(j)} \rangle = \frac{l}{3} r_j^{2l-2} \delta_{ll'} \delta_{mm'}, \quad (8) \\ \langle \psi_{lm}^{(j)*} \psi_{l'm'}^{(j)} \rangle = \frac{1}{3} \frac{l+1}{r_j^{2l+4}} \delta_{ll'} \delta_{mm'}, \quad \langle \chi_{lm}^{(j)*} \psi_{l'm'}^{(j)} \rangle = 0,$$

where brackets stand for angular and orientational averaging. Note that, for QEs with random dipole orientations and uniformly distributed in the shell, the direct term D_{jk}^0 in system (5) vanishes on average, so we keep only the plasmon term D_{jk}^p in the following.

III. COLLECTIVE MODES OF QUANTUM EMITTERS AND SPASER CONDITION

Within semiclassical approach, the first (homogeneous) equation in the system (3) determines the spaser condition. We now transform it from individual QE representation to collective mode representation by introducing collective polarizations as

$$\rho_\lambda = \sum_{j=1}^M \psi_\lambda^{(j)*} \rho_j, \quad (9)$$

where $\lambda = (lm)$ is composite mode index. Keeping only the plasmon term D_{jk}^p in the coupling matrix, multiplying the first equation by $\psi_\lambda^{(j)*}$ and summing over j , the system (3) takes the form

$$(\omega - \omega_{21} + i/\tau_2) \rho_\lambda - \sum_{\lambda'} S_{\lambda\lambda'} \alpha_{\lambda'} \rho_{\lambda'} = 0, \\ N - \bar{N} + \frac{4\tau_1\mu^2}{\hbar} \sum_{\lambda} \alpha_\lambda''(\omega) |\rho_\lambda|^2 = 0, \quad (10)$$

where $N = \sum_j n_j$ is gain population inversion, $\bar{N} = \bar{n}M$ is that due to the pump, and

$$S_{\lambda\lambda'} = \frac{\mu^2}{\hbar} \sum_{j=1}^M \psi_\lambda^{(j)*} n_j \psi_{\lambda'}^{(j)} \quad (11)$$

is the mode coupling matrix.

Single mode approximation

Let us perform angular and orientational averaging in system (10). In the leading order in $1/M$, this is done by replacing the mode coupling matrix S with its average using relations (8),

$$\langle S_{\lambda\lambda'} \rangle = s_l \delta_{ll'} \delta_{mm'}, \quad s_l = \frac{l+1}{3} \frac{\mu^2}{\hbar} \sum_j \frac{n_j}{r_j^{2l+4}}, \quad (12)$$

yielding the consistency condition for each mode

$$\omega - \omega_{21} + i/\tau_2 = s_l \alpha_l(\omega). \quad (13)$$

The real and imaginary parts of Eq. (13) determine, respectively, the spaser frequency and threshold population inversion:

$$\omega - \omega_{21} = s_l \alpha_l'(\omega), \quad \tau_2 s_l \alpha_l''(\omega) = 1. \quad (14)$$

By taking their ratio, the spasing frequency ω_s is determined from a simple equation

$$\tau_2(\omega - \omega_{21}) = \frac{\alpha_l'(\omega)}{\alpha_l''(\omega)}. \quad (15)$$

Note that since Eqs. (14) are independent of azimuthal number m , each l -mode is $(2l+1)$ -fold degenerate.

Assume now that gain molecules are uniformly distributed in a thin layer at approximately equal distance d from the metal NP surface (e.g., on top of dielectric shell), so that the averaged coupling (12) takes the form

$$s_l = \frac{\mu^2}{\hbar} \frac{(l+1)N}{3(R+d)^{2l+4}}, \quad (16)$$

For QE frequency ω_{21} close to the l -pole plasmon resonance frequency ω_l , the NP polarizability can be expanded near the plasmon pole as

$$\alpha_l(\omega) = \frac{B_l}{\omega_l - \omega - i/\tau_l}, \quad (17)$$

where $\tau_l = [\partial \varepsilon'(\omega_l)/\partial \omega_l]/\varepsilon''(\omega_l)$ is plasmon lifetime and coefficient B_l depends on NP shape and composition [15]. For spherical NP, B_l is obtained from Eq. (6) as

$$B_l = \frac{(2l+1)\varepsilon_d R^{2l+1}}{l \partial \varepsilon'(\omega_l)/\partial \omega_l}. \quad (18)$$

With NP polarization in the form (17), we obtain from Eq. (15) the standard spaser frequency

$$\omega_0 = \frac{\tau_l \omega_l + \tau_2 \omega_{21}}{\tau_l + \tau_2}, \quad (19)$$

while the second equation in system (14) determines, for $|\omega_l - \omega_{21}| \tau_l \ll 1$, the population inversion *threshold* N_0 ,

$$\frac{\mu^2 \tau_2}{\hbar} \frac{(2l+1)(l+1)}{3l \varepsilon''(\omega_l)} \frac{N_0 R^{2l+1}}{(R+d)^{2l+4}} = 1. \quad (20)$$

Note that N_0 increases exponentially for large- l modes.

IV. MODE MIXING AND SPASER QUENCHING

While in the absence of gain, different plasmon modes are orthogonal, the presence of QEs with random positions and orientations violates the underlying NP symmetry and leads to mode mixing. For large number M of QEs uniformly distributed around the NP, the spherical symmetry is preserved *on average*, so that single-mode description is reasonably accurate, while corrections due to mode mixing are suppressed by factor of $1/M$. However, for QEs located close to NP surface, the coupling to nonresonant modes is strong, so that even weak inhomogeneity of QE distribution can lead to significant mode mixing effects. Below we analyze the effect of mode mixing on spaser condition and establish a simple criteria, in terms of system parameters, for the validity of single-mode description.

A. Quenching onset

We assume that QE frequency ω_{21} is tuned to the dipole plasmon mode ($l = 1$) frequency ω_1 , and incorporate the effect of higher ($l > 1$) nonresonant modes as follows. First, we separate out the resonant and higher-order modes in the first equation of system (10) by splitting it into two equations,

$$\begin{aligned}\Omega\rho_1 - S_{11}\alpha_1\rho_1 - \sum_{\lambda} S_{1\lambda}\alpha_{\lambda}\rho_{\lambda} &= 0, \\ \Omega\rho_{\lambda} - S_{\lambda 1}\alpha_1\rho_1 - \sum_{\lambda'} S_{\lambda\lambda'}\alpha_{\lambda'}\rho_{\lambda'} &= 0,\end{aligned}\quad (21)$$

where we denoted $\Omega = \omega - \omega_{21} + i/\tau_2$, and the indexes λ and λ' do *not* include the resonant mode. In the first order in $1/M$, we include the coupling of resonant mode with nonresonant modes, but disregard nonresonant modes' coupling with each other. After replacing the matrix $S_{\lambda\lambda'}$ in the second equation by its average (12), the polarization for nonresonant modes can be expressed via that for the resonance mode as

$$\rho_{\lambda} = \frac{S_{\lambda 1}\alpha_1}{\Omega - s_{\lambda}\alpha_{\lambda}} \rho_1. \quad (22)$$

Then, eliminating ρ_{λ} from the first equation of system (21), we obtain the consistency condition [restoring indexes (lm)],

$$\Omega\delta_{mm'} - \left(S_{1m,1m'} + \sum_{l_1 m_1} ' \frac{S_{1m,l_1 m_1}\alpha_{l_1} S_{l_1 m_1,1m'}}{\Omega - s_{l_1}\alpha_{l_1}} \right) \alpha_1 = 0, \quad (23)$$

where the sum runs over $l_1 > 1$ and m_1 in the interval $(-l_1, l_1)$, while m, m' take values $(-1, 0, 1)$. Performing angular and orientational averaging in Eq. (23) (see Appendix A), we obtain the spaser condition in the form

$$\omega - \omega_{21} + i/\tau_2 - s_1\alpha_1(\omega) [1 + f(\omega)] = 0, \quad (24)$$

where the function

$$f(\omega) = \frac{1}{5M} \sum_{l>1} \frac{(11l+7)s_l\alpha_l(\omega)}{\omega - \omega_{21} + i/\tau_2 - s_l\alpha_l(\omega)} \quad (25)$$

includes the coupling to high- l modes. In the absence of such coupling ($f = 0$), the solutions of Eq. (25) for spaser frequency ω_0 and threshold population N_0 are given, respectively, by Eqs. (19) and (20). In the presence of coupling, the corresponding solutions ω and N deviate from ω_0 and N_0 by the amount depending on distance d to the NP surface. While for $d \gtrsim R$, the coefficients s_l , given by Eq. (16), change rapidly with d , for $d \ll R$ they are only weakly dependent on d , indicating that, in this case, the main contribution to f comes from multitude of modes with large l . To estimate the characteristic distance d below which high- l modes become important, we note that, for nonresonant modes we have $\tau_2 s_l \alpha_l \ll 1$ and

so the last term in denominator of Eq. (25) can be disregarded. Since the main contribution comes from high- l terms, so we can replace α_l by $R^{2l+1}[\varepsilon(\omega) - \varepsilon_d]/[\varepsilon(\omega) + \varepsilon_d]$ [see Eq. (6)] and write

$$f(\omega) = \frac{\mu^2}{15\hbar} \frac{N}{M} \frac{\varepsilon(\omega) - \varepsilon_d}{\varepsilon(\omega) + \varepsilon_d} \frac{g}{\omega - \omega_{21} + i/\tau_2}, \quad (26)$$

where

$$g = \sum_{l>1} (11l+7)(l+1) \frac{R^{2l+1}}{(R+d)^{2l+4}}. \quad (27)$$

For $d/R \ll 1$, replacing the sum over l by the integral, we obtain $g \approx 11/4d^3$. For small deviations of ω from the plasmon frequency, i.e., $\varepsilon(\omega) \approx \varepsilon(\omega_1) = -2\varepsilon_d$, and using that $(\omega - \omega_{21})\tau_2 \ll 1$, we finally obtain

$$|f| \approx \frac{\mu^2 \tau_2}{2\hbar d^3} \frac{N}{M}. \quad (28)$$

The onset of quenching corresponds to $|f| \sim 1$. In the first order, replacing N with $N_0 = R^3 \varepsilon''(\omega_1) \hbar / 2\mu^2 \tau_2$ from Eq. (20), we arrive at the estimate for onset value of d :

$$d \sim R \left[\frac{\varepsilon''(\omega_1)}{4M} \right]^{1/3}. \quad (29)$$

For example, for $M \sim 10^3$ and with $\varepsilon''(\omega_1) \approx 2$ for spherical Au NP, the mode mixing is important for $d/R \lesssim 0.1$.

B. Numerical results

Below we present the results of numerical calculations for spherical Au NP of radius R and M QEs randomly distributed on top of dielectric shell at distance d from the metal surface with frequencies ω_{21} tuned to the dipole plasmon resonance frequency ω_1 . In all calculations, we used experimental Au dielectric function [57] and included modes with angular momenta up to $l_{\max} = 50$. Note that we excluded the region of very small distances dominated by quantum effects, which are out of scope of this paper [58].

In Fig. 2, we plot the spaser frequency ω and population inversion threshold N vs. gain-NP distance d (see inset) obtained by solving Eq. (24) for several ensemble sizes. To highlight the role of nonresonant modes, we show the deviations of ω and N from the corresponding values ω_0 and N_0 for resonant mode coupling only (i.e., $f = 0$). For small distances $d/R \ll 1$, the effect of nonresonant modes can be substantial depending on the ensemble size, consistent with our estimate (29). With decreasing d , the spaser frequency ω shifts upwards (high-order modes have larger frequencies), and so does threshold N to compensate the energy leakage to nonresonant modes not participating in the feedback. At the

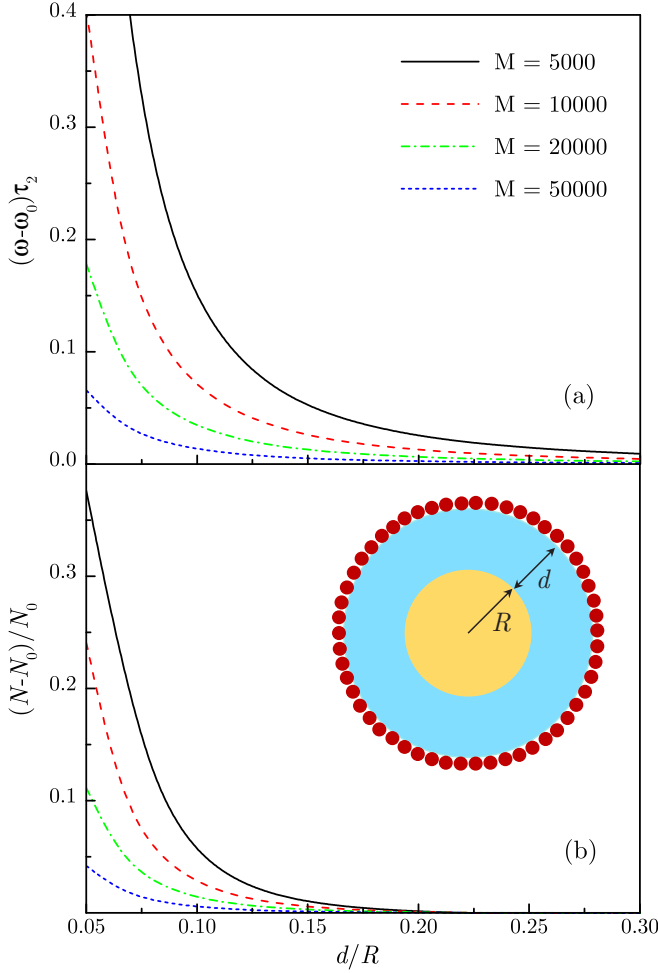


FIG. 2. (a) Spaser frequency shift and (b) relative population inversion threshold shift are shown vs. shell thickness for several QE ensemble sizes. Inset: Schematics of QEs distributed on top of composite NP.

same time, with increasing ensemble size M , the deviations of spaser frequency and of threshold population inversion from their single-mode values are significantly reduced, indicating restoration of spherical symmetry as fluctuations of the QE distribution diminish.

Note that the overall effect of nonresonant modes on spaser action is significantly weaker than on single-QE fluorescence. The calculated quantum efficiency Q , shown in Fig. 1 (see Appendix B for detail), falls below 20% at distances $d \sim R$, and it is even lower for smaller NPs, indicating that fluorescence is largely quenched at such distances. In contrast, spaser quenching become substantial only for (average) gain-NP separations well below NP size (see Fig. 2), while for larger distances, spaser quenching is largely suppressed.

Finally, we considered here a specific setup with all QEs distributed at about equal distance to the metal NP, e.g., on top of dielectric shell. Such configuration provides us with better control over gain coupling to nonresonant modes and allows straightforward comparison with the single QE radiation quenching near the metal

surface. In a more common setup, gain is distributed within some region with volume comparable or exceeding the metal volume, e.g., within the dielectric shell, implying that only a relatively small fraction of QEs, located sufficiently close to the surface, can undergo energy exchange with higher-order modes, whose electric fields decay rapidly outside the metal structure. Therefore, for a given gain concentration, extending the gain region size should lower the spaser threshold by suppressing quenching effects.

V. CONCLUSIONS

In summary, we studied the effect of energy transfer between gain and nonresonant plasmon modes on spaser action. We found that mode mixing, originating from inhomogeneity of gain distribution, interferes with the feedback mechanism and leads to the upward shift of spaser frequency and population inversion threshold. We have shown that these quenching effects are restricted to a thin layer near the metal surface, and are suppressed for large gain concentration. We established a simple criteria relating quenching onset with gain concentration supported by numerical calculations for core-shell NP based spasers.

ACKNOWLEDGMENTS

This work was supported in part by the National Science Foundation under grants No. DMR-1610427 and No. HRD-1547754.

Appendix A: Averaging

The angular and orientations averaging of Eq. (23) renders $m = m'$, so we set $m' = m$ and sum over m . In the products $\psi_{1m}^{(j)*} \psi_{l_1 m_1}^{(j)} \psi_{l_1 m_1}^{(k)*} \psi_{1m}^{(k)}$ appearing in $S_{1m, l_1 m_1} S_{l_1 m_1, 1m}$ only the terms with $j = k$ survive the averaging since $l_1 > 1$, thus reducing the result by factor $1/M$. The averaging over orientations is performed using the relation

$$\langle \mathbf{e}_j^\alpha \mathbf{e}_j^\beta \mathbf{e}_j^\gamma \mathbf{e}_j^\delta \rangle = \frac{1}{15} (\delta_{\alpha\beta} \delta_{\gamma\delta} + \delta_{\alpha\gamma} \delta_{\beta\delta} + \delta_{\alpha\delta} \delta_{\beta\gamma}) \quad (\text{A1})$$

and Eq. (23) takes the form

$$\Omega - \left(s_1 + \sum_{l>1} \frac{\alpha_l f_l}{\Omega - s_l \alpha_l} \right) \alpha_1 = 0, \quad (\text{A2})$$

where

$$f_l = \frac{1}{45} \left(\frac{\mu^2}{\hbar} \right)^2 \sum_{j=1}^M n_j^2 \left[J_1 J_l + 2 \left(J_1^r J_l^r + J_1^\theta J_l^\theta + J_1^\phi J_l^\phi \right) \right]. \quad (\text{A3})$$

Here we defined

$$J_l^\alpha = \frac{4\pi}{2l+1} \sum_{m=-l}^l \nabla_\alpha \left[\frac{Y_{lm}(\hat{\mathbf{r}})}{r^{l+1}} \right] \nabla_\alpha \left[\frac{Y_{lm}(\hat{\mathbf{r}})}{r^{l+1}} \right], \quad (\text{A4})$$

and $J_l = J_l^r + J_l^\theta + J_l^\phi$. Using elementary properties of spherical harmonics we find

$$J_l^r = \frac{(l+1)^2}{r^{2l+4}}, \quad J_l^\theta = J_l^\phi = \frac{l(l+1)}{2r^{2l+4}}, \quad J_l = \frac{(2l+1)(l+1)}{r^{2l+4}}, \quad (\text{A5})$$

yielding

$$f_l = \frac{2}{45}(l+1)(11l+7) \left(\frac{\mu^2}{\hbar} \right)^2 \sum_{j=1}^M \frac{n_j^2}{r_j^6 r_j^{2l+4}}. \quad (\text{A6})$$

For weak dispersion of radial distribution, $r_j \approx r$ and weak inhomogeneity in molecular population inversion, $n_j \approx n = N/M$, we obtain

$$f_l = \frac{1}{5M}(11l+7)s_1 s_l, \quad (\text{A7})$$

with s_l given by Eq. (16), which, after being substituted into Eq. (A2), leads to Eq. (24).

Appendix B: Fluorescence quantum efficiency

Fluorescence quantum efficiency for a single QE near metal NP has the form

$$Q = \frac{\Gamma_r}{\Gamma_r + \Gamma_{nr}}, \quad (\text{B1})$$

where Γ_r and Γ_{nr} are, respectively, radiative and non-radiative decay rates. For a QE oriented normally to spherical NP surface, these rates have the form [20–23]

$$\Gamma_r = \gamma_r^0 \left| 1 + \frac{2\alpha_1(\omega_1)}{(R+d)^3} \right|^2, \quad \Gamma_{nr} = \frac{3\gamma_r^0}{2k^3} \sum_l \frac{(l+1)^2 \alpha_l''(\omega_1)}{(R+d)^{2l+4}}, \quad (\text{B2})$$

where γ_r^0 is the radiative decay rate for isolated QE and k is the light wave-vector. T

-
- [1] D. Bergman and M. I. Stockman, Phys. Rev. Lett., **90**, 027402, (2003).
 - [2] M. I. Stockman, Nature Photonics, **2**, 327, (2008).
 - [3] M. I. Stockman, J. Opt. **12**, 024004, (2010).
 - [4] M. A. Noginov, G. Zhu, A. M. Belgrave, R. Bakker, V. M. Shalaev, E. E. Narimanov, S. Stout, E. Herz, T. Suteewong and U. Wiesner, Nature, **460**, 1110, (2009).
 - [5] R. F. Oulton, V. J. Sorger, T. Zentgraf, R.-M. Ma, C. Gladden, L. Dai, G. Bartal, and X. Zhang, Nature **461**, 629, (2009).
 - [6] E. Plum, V. A. Fedotov, P. Kuo, D. P. Tsai, and N. I. Zheludev, Opt. Expr. **17**, 8548, (2009).
 - [7] R. Ma, R. Oulton, V. Sorger, G. Bartal, and X. Zhang, Nature Mater., **10**, 110, (2010).
 - [8] K. Ding, Z. C. Liu, L. J. Yin, M. T. Hill, M. J. H. Marel, P. J. van Veldhoven, R. Netzel, and C. Z. Ning, Phys. Rev. B **85**, 041301(R) (2012).
 - [9] Y.-J. Lu, J. Kim, H.-Y. Chen, C. i Wu, N. Dabidian, C. E. Sanders, C.-Y. Wang, M.-Y. Lu, B.-H. Li, X. Qiu, W.-H. Chang, L.-J. Chen, G. Shvets, C.-K. Shih, and S. Gwo, Science **337**, 450 (2012).
 - [10] W. Zhou, M. Dridi, J. Y. Suh, C. H. Kim, D. T. Co, M. R. Wasielewski, G. C. Schatz, and T. W. Odom, Nat. Nano. **8**, 506 (2013).
 - [11] X. Meng, A. V. Kildishev, K. Fujita, K. Tanaka, and V. M. Shalaev, Nano Lett. **13**, 4106, (2013).
 - [12] Y. Lu, C.-Y. Wang, J. Kim, H.-Y. Chen, M.-Y. Lu, Y.-C. Chen, W.-H. Chang, L.-J. Chen, M. I. Stockman, C.-K. Shih, S. Gwo, Nano Lett. **14**, 4381 (2014).
 - [13] R.-M. Ma, S. Ota, Y. Li, S. Yang, and X. Zhang, Nat. Nano. **9**, 600 (2014).
 - [14] A. Yang, T. B. Hoang, M. Dridi, C. Deeb, M. H. Mikkelsen, G. C. Schatz, and T. W. Odom, Nat. Comm. **6**, 6939 (2015).
 - [15] M. I. Stockman, in *Plasmonics: Theory and Applications*, edited by T. V. Shahbazy and M. I. Stockman (Springer, New York, 2013).
 - [16] V. Apalkov and M. I. Stockman, Light: Science & Applications **3**, e191 (2014).
 - [17] C. Rupasinghe, I. D. Rukhlenko, and M. Premaratne, ACS Nano, **8** 2431 (2014).
 - [18] V. N. Pustovit, A. M. Urbas, and D. E. Zelmon, Phys. Rev. B **94**, 235445 (2016).
 - [19] M. Premaratne and M. I. Stockman, Adv. Opt. Phot. **9**, 79 (2017).
 - [20] J. Gersten and A. Nitzan, J. Chem. Phys. **75**, 1139 (1981).
 - [21] R. Rupp, J. Chem. Phys. **76**, 1681 (1982).
 - [22] V.N. Pustovit and T. V. Shahbazy, Phys. Rev. Lett., **102**, 077401, (2009).
 - [23] V.N. Pustovit and T. V. Shahbazy, Phys. Rev. B, **82**, 075429, (2010).
 - [24] E. Dulkeith, A. C. Morteau, T. Niedereichholz, T. A. Klar, J. Feldmann, S. A. Levi, F. C. J. M. van Veggel, D. N. Reinhoudt, M. Moller, and D. I. Gittins, Phys. Rev. Lett. **89**, 203002 (2002).
 - [25] C. D. Geddes and J. R. Lakowicz, J. Fluoresc. **12**, 121 (2002).
 - [26] O. Kulakovich, N. Strekal, A. Yaroshevich, S. Maskevich, S. Gaponenko, I. Nabiev, U. Woggon, and M. Artemyev, Nano Lett. **2**, 1449 (2002).
 - [27] Z. Gueroui, and A. Libchaber, Phys. Rev. Lett. **93**, 166108 (2004).
 - [28] E. Dulkeith, M. Ringler, T. A. Klar, J. Feldmann, A. M. Javier, and W. J. Parak, Nano Lett. **5**, 585 (2005).
 - [29] N. Liu, B. S. Prall, and V. I. Klimov, J. Am. Chem. Soc. **128**, 15362 (2006).
 - [30] T. L. Jennings, M. P. Singh, and G. F. Strouse, J. Am. Chem. Soc. **128**, 5462 (2006).

- [31] H. Mertens, J. S. Biteen, H. A. Atwater, and A. Polman, *Nano Lett.* **6**, 2622 (2006).
- [32] P. P. Pompa, L. Martiradonna, A. D. Torre, F. D. Sala, L. Manna, M. De Vittorio, F. Calabi, R. Cingolani, and R. Rinaldi, *Nature Nanotech.* **1**, 126 (2006).
- [33] P. Anger, P. Bharadwaj, and L. Novotny, *Phys. Rev. Lett.* **96**, 113002 (2006).
- [34] S. Kuhn, U. Hakanson, L. Rogobete, and V. Sandoghdar, *Phys. Rev. Lett.* **97**, 017402 (2006).
- [35] P. Bharadwaj and L. Novotny, *Opt. Express* **17**, 14266 (2007).
- [36] J. Seelig, K. Leslie, A. Renn, S. Klühn, V. Jacobsen, M. van de Corput, C. Wyman, and V. Sandoghdar, *Nano Lett.* **7**, 685 (2007).
- [37] K. Aslan, M. Wu, J. R. Lakowicz, and C. D. Geddes, *J. Am. Chem. Soc.* **129**, 1524 (2007).
- [38] Y. Chen, K. Munechika, and D. S. Ginger, *Nano Lett.* **7**, 690 (2007).
- [39] J. Zhang, Y. Fu, M. H. Chowdhury, and J. R. Lakowicz, *Nano Lett.* **7**, 2101 (2007).
- [40] F. Tam, G. P. Goodrich, B. R. Johnson, and N. J. Halas, *Nano Lett.*, **7**, 496 (2007).
- [41] A. Bek, R. Jansen, M. Ringler, S. Mayilo, T. A. Klar, and J. Feldmann, *Nano Lett.* **8**, 485 (2008).
- [42] R. Bardhan, N. K. Grady, J. R. Cole, A. Joshi, and N. J. Halas, *ACS Nano* **3**, 744 (2009).
- [43] T. Ming, L. Zhao, Z. Yang, H. Chen, L. Sun, J. Wang, and C. Yan, *Nano Lett.* **9**, 3896 (2009).
- [44] A. Kinkhabwala, F. Z. Yu, S. H. Fan, Y. Avlasevich, K. Mullen and W. E. Moerner, *Nature Photon.* **3**, 654 (2009).
- [45] P. Viste, J. Plain, R. Jaffiol, A. Vial, P. M. Adam, and P. Royer, *ACS Nano* **4**, 759 (2010).
- [46] Y. Fu, J. Zhang, and J. R. Lakowicz, *J. Am. Chem. Soc.* **132**, 5540 (2010).
- [47] K. Munechika, Y. Chen, A. F. Tillack, A. P. Kulkarni, I. J.-L. Plante, A. M. Munro, and D. S. Ginger, *Nano Lett.* **10**, 2598 (2010).
- [48] T. Ming, L. Zhao, H. Chen, K. C. Woo, J. Wang, and H.-Q. Lin, *Nano Lett.* **11**, 2296 (2011).
- [49] D. Ratchford, F. Shafiei, S. Kim, S. K. Gray, and X. Li, *Nano Lett.* **11**, 1049 (2011).
- [50] G. Rainó, T. Stoferle, C. Park, H.-C. Kim, T. Topuria, P. M. Rice, I.-J. Chin, R. D. Miller, and R. F. Mahrt, *ACS Nano* **5**, 3536 (2011).
- [51] M. Wegener, J. L. Garcia-Pomar, C. M. Soukoulis, N. Meinzer, M. Ruther, and S. Linden, *Opt. Express* **16**, 19785 (2008).
- [52] N. Arnold, B. Ding, C. Hrelescu, and T. A. Klar, *Beilstein J. Nanotechnol.* **4**, 974 (2013).
- [53] X.-L. Zhong and Z.-Y. Li, *Phys. Rev. B* **88**, 085101 (2013).
- [54] D. G. Baranov, E. S. Andrianov, A. P. Vinogradov, and A. A. Lisyansky, *Opt. Express* **21**, 10779 (2013).
- [55] V. G. Bordo *Phys. Rev. A* **88**, 013803 (2013).
- [56] V. N. Pustovit, A. M. Urbas, A. V. Chipouline, and T. V. Shahbazyan, *Phys. Rev. B* **93**, 165432 (2016).
- [57] P. B. Johnson and R. W. Christy, *Phys. Rev. B*, **6**, 4370, (1973).
- [58] V. N. Pustovit and T. V. Shahbazyan, *J. Chem. Phys.* **136**, 204701 (2012).